https://doi.org/10.5194/tc-2023-111
Preprint. Discussion started: 3 August 2023

The Cryosphere Discussions

Snow accumulation, albedo and melt patterns following road construction on permafrost, Inuvik-Tuktoyaktuk Highway, Canada

Jennika Hammar[1], Inge Grünberg[1], Steve V. Kokelj[2], Jurjen van der Sluijs[3], and Julia Boike[1,4]

[1]Permafrost Research Section, Alfred Wegener Institute Helmholtz Centre for Polar and Marine Research, Potsdam, Germany
[2]Northwest Territories Geological Survey, Government of Northwest Territories, Yellowknife, NT X1A 2L9, Canada
[3]NWT Centre for Geomatics, Government of Northwest Territories, Yellowknife, NT X1A 2L9, Canada
[4]Geography Department, Humboldt-Universität zu Berlin, Berlin, Germany

Correspondence: Jennika Hammar (jennika.hammar@awi.de)

Abstract

Roads constructed on permafrost can have a significant impact on the surrounding environment, potentially inducing permafrost degradation. These impacts arise from factors such as snow accumulation near the road, which affects the soil's thermal and hydrological regime and road dust that decreases the snow's albedo, altering the timing of snowmelt. However, our current understanding of the magnitude and the spatial extent of these effects is limited. In this study we addressed this gap by using remote sensing techniques to assess the spatial effect of the Inuvik to Tuktoyaktuk Highway (ITH) in Northwest Territories, Canada, on snow accumulation, snow albedo and snowmelt patterns. We quantified the snow accumulation at road segments in the Trail Valley Creek area using digital elevation model differencing. We found increased snow accumulation up to 36 m from the road center. The magnitude of this snow accumulation was influenced by the prevailing wind direction and the height of the embankment. Furthermore, by analysing 43 Sentinel-2 satellite images between February and May 2020 we observed reduced snow albedo values within 500 m of the road, resulting in a twelve days earlier onset of snowmelt within 100 m from the road. We examined snowmelt patterns before, during and after the road construction using the normalized difference snow index from Landsat-7 and Landsat-8 imagery. Our analysis revealed that the road affected the snowmelt pattern up to 600 m from the road, even in areas which appeared undisturbed. In summary, our study improves our understanding of the spatial impact of gravel roads on permafrost on snow cover accumulation, snow albedo and snowmelt patterns. Our study underscores important contribution that remote sensing can provide to improve our understanding of the effects of infrastructure development on permafrost environments.

1 Introduction

Roads constructed on permafrost are at great risk due to the intense climate warming in the Arctic (Rantanen et al., 2022). While climate warming is inducing permafrost thaw at the global scale (Biskaborn et al., 2019), infrastructure may enhance permafrost degradation at the local scale. Arctic highways alter the local environment, leading to snow accumulation, water

https://doi.org/10.5194/tc-2023-111
Preprint. Discussion started: 3 August 2023

ponding at the embankment toe and dust deposition which are key processes driving permafrost degradation along Arctic highways (Benson et al., 1975; O'Neill and Burn, 2017; Schneider von Deimling et al., 2021). Ground subsidence caused by warming or road effects can have a severe impact on infrastructure leading to increased costs for road maintenance and risk of road failure (Nelson et al., 2001). However, as a result of climate change's impact on winter road accessibility (Gädeke et al., 2021) and the increasing resource development in northern regions, there has been a surge in infrastructure construction. Over 175 infrastructure projects have been funded in the Northwest Territories, Canada since 2002. $57\,\%$ of these projects are related to roads and highways (Government of Canada, 2021).

Snow drifting in the lee of the road and winter road maintenance lead to snow accumulation at the toe of the embankment (Benson et al., 1975; O'Neill and Burn, 2017). The thermal conductivity of snow, which is low and primarily determined by its density, can range from less than $0.10\,\mathrm{Wm^{-1}K^{-1}}$ for loosely packed, fresh snow to over $0.50\,\mathrm{Wm^{-1}K^{-1}}$ for densely packed and ripened snow (Zhang, 2005). This is five to twenty times lower than the thermal conductivity of mineral soil (Zhang, 2005). Consequently, snow is an effective insulator and prevents the soil from cooling during the winter months (Darrow, 2011; Fortier et al., 2011). However, the insulating effect of snow depends on its depth, timing and duration of snow accumulation. A thin snow cover may cool off the underlying soil because of the high albedo and emissivity of snow (Zhang, 2005) while the insulating effect prevails with increased snow depth (Ge and Gong, 2010), leading to increased soil temperature and thaw depths (Idrees et al., 2015; Park et al., 2015; O'Neill and Burn, 2017). Process-based land surface models showed that variation in ground heat loss, refreezing of the active layer and permafrost thaw are most strongly affected by early season snow accumulation (Park et al., 2015).

Arctic highways alter the patterns of snow accumulation, but also affect the snow cover in other ways. In particular, gravel road construction, maintenance and traffic create dust, which settles on the surrounding terrain. The dust deposition is influenced by the wind direction and decreases logarithmically from the road (Everett, 1980; Walker et al., 2022). During the snow season, road dust reduces the snow albedo, particularly when dust particles accumulate at the snow surface during snowmelt. This results in an earlier spring snowmelt and, consequently, earlier soil thaw close to the road (Walker and Everett, 1987).

Due to global warming, the coverage of shrubs has increased and lichen cover has declined in the greater Mackenzie Delta Region of the western Canadian Arctic (Fraser et al., 2014; Nill et al., 2022). This phenomenon can be exacerbated by the presence of roads, as shrubs with relatively low nutrient use efficiencies are favored due to the increased soil nutrient availability resulting from dust deposition and increased soil moisture (Gill et al., 2014; Cameron and Lantz, 2016). As shrubs act as a windbreak, increased shrub growth alters the snow thickness and density and thus the insulating effect of the snow cover (Ackerman, 2018). Tall shrubs also reduce the availability of light, water and nutrients for mosses, while heavy dust deposition eradicates low-growing mosses and lichens (Raynolds et al., 2014). This, in turn, results in a decline in moss and lichen cover, which may decrease thermal insulation of the ground in summer, further amplifying soil warming.

In the present study, we focus on the Inuvik to Tuktoyaktuk Highway (ITH) in Northwest Territories, Canada (NWT). The highway corridor traverses the ecoclimate gradient of the treeline characterized by a northward decrease in snow and permafrost temperatures (Kokelj et al., 2017) and is characterized by a heterogeneous topography and ice-rich permafrost which is particularly vulnerable to climate change (Rampton, 1988; Burn and Kokelj, 2009). The highway was only recently

https://doi.org/10.5194/tc-2023-111
Preprint. Discussion started: 3 August 2023

constructed and therefore provides a unique opportunity to study its impacts on ice-rich and thaw sensitive permafrost from the beginning.

In situ measurements, including snow depth or albedo, help to derive important information on processes locally. However, such local information may not be applicable or extendable to another section of the road. At the date of writing, we are not aware of any other studies that have quantified the snow accumulation enhancement along a permafrost gravel road with other methods than point-wise snow depth measurements (Benson et al., 1975; O'Neill and Burn, 2017). However, point observations are limited to few transects with limited maximum distance to the road. Drone imaging have been successfully used to determine snow depth using structure from motion techniques (Wilcox et al., 2019; Walker et al., 2021). In addition, the use of drone imaging techniques has facilitated the observation and quantification of permafrost processes and infrastructure impacts due to thaw near infrastructure (van der Sluijs et al., 2018). Rapid advances in drone technology have expanded applications beyond line-of-sight (Van der Sluijs et al., 2023 in press) comparable with conventional light detection and ranging (LiDAR) coverage. However, to our knowledge, drone-based mapping has not yet been used to assess snow accumulation along Arctic highways and LiDAR data is typically only collected in summer for infrastructure and thermokarst mapping (van der Sluijs et al., 2018).

Passive satellite microwave-based estimates of snow depth are generally too coarse with spatial resolutions of $25\,\mathrm{km}$ and a saturation of around $0.8\,\mathrm{m}$ snow depth, which limits the usability for applications where higher spatial resolutions are required (Lievens et al., 2022). Compared to drones, satellite remote sensing offers the advantage of wider spatial coverage and longer time series, enabling the retrieval of physical surface parameters that serve as indicators of permafrost degradation at larger scales. Snow cover percentage can be well studied by optical remote sensing because of its spectral properties, making it distinguishable from snow-free areas (e.g. Hall et al., 1995; Macander et al., 2015; Morse and Wolfe, 2015).

Our study utilized remote sensing techniques to investigate the effects of the ITH on snow conditions. We analyzed snow depth, snow albedo and snowmelt patterns using LiDAR data, Sentinel-2 satellite imagery, and Landsat data. The specific objectives of this paper are to (1) quantify the influence of embankment height and aspect on snow accumulation, (2) assess the impact of road dust on snow albedo and its variation with distance from the road and (3) determine how road dust impacts snowmelt patterns along the road corridor before, during, and after road construction.

2 Datasets & Methods

2.1 Study site

Our study site was the ITH, which is a $138\,\mathrm{km}$ all-weather gravel highway to the east of the Mackenzie Delta in Northwest Territories, Canada (Fig. 1). The highway's construction began in 2014 and it was officially opened in 2017. In order to protect the underlying thaw-sensitive permafrost, the highway was constructed with an embankment that had a minimum design thickness of 1.3 m (Kiggiak - EBA, 2011). This was designed to accommodate consolidation of the initially frozen embankment with the intent of maintaining an active layer above the native permafrost. This embankment included the $8\,\mathrm{m}$ to $9\,\mathrm{m}$ wide highway and slopes of $33\,\%$ on both sides. The embankment height varies along the road depending on the topography

https://doi.org/10.5194/tc-2023-111
Preprint. Discussion started: 3 August 2023

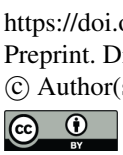

and ice content (Kiggiak - EBA, 2011). Moreover, the highway was built using fill but no cuts to minimize the disturbance of the permafrost (Kiggiak - EBA, 2011). Since its official opening, ongoing maintenance efforts have been undertaken on the road to address ground subsidence and embankment settlement. These maintenance activities have involved the replacement and installation of culverts, as well as regular grading to ensure a passable surface is maintained.

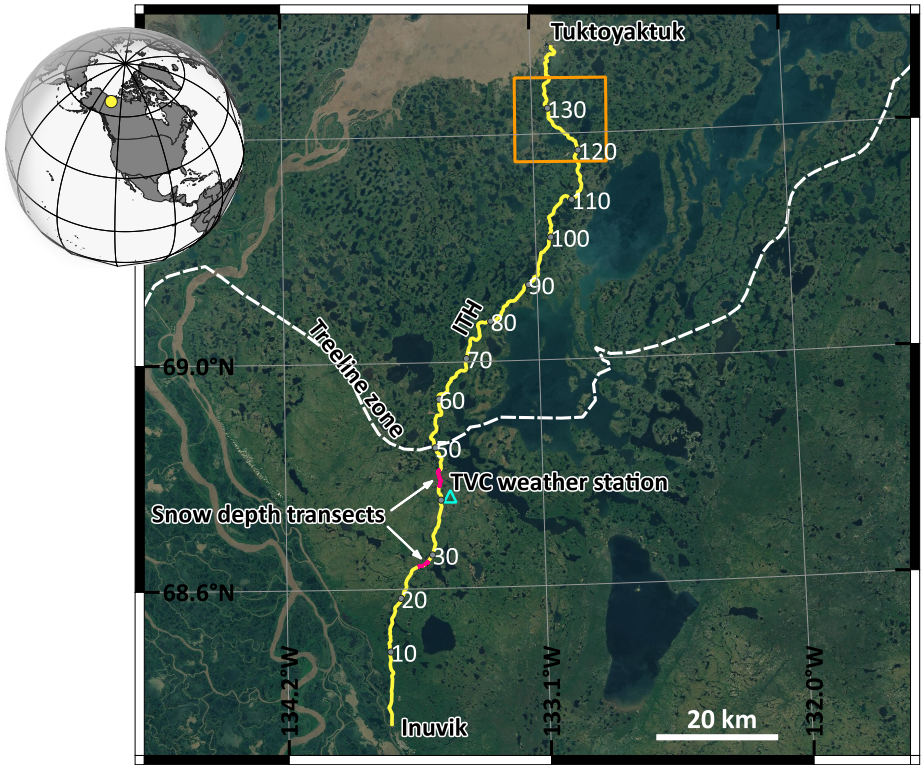

Figure 1. The Inuvik–Tuktoyaktuk Highway (ITH) in Northwest Territories, Canada with kilometers shown as white numbers. The location of the snow accumulation analysis close to Trail Valley Creek (TVC) research station is highlighted in red (at km 27, 28 and 42.5–45.5). The inset map at the top left depicts the location of the study area in North America and the orange square highlights the example chosen for the snow cover image in Fig. 6a–b. The treeline zone (Brandt, 2009) is shown as white dashed line. Base map: Sentinel-2 cloudless data by EOX IT Services GmbH.

ITH is located within the continuous permafrost zone uplands east of the Mackenzie Delta and traverses the treeline through the physiographic regions the Anderson Plain in the south and Tuktoyaktuk Coastlands in the north (Mackay, 1963; Rampton, 1988). The region south of the taiga–tundra transition zone is characterized by open spruce woodlands and peat plateaus. Tree cover decreases northwards and transforms to tundra with tall shrubs at the southern edge of the transition zone and sedges and dwarf shrubs at the northern edge of the transition zone (Burn and Kokelj, 2009). Sedges, grasses, ericaceous shrubs and lichens dominate the low arctic tundra north of the treeline (Burn and Kokelj, 2009). The landscape is characterized by a lake-rich, hummocky and rolling terrain. The subsurface material predominantly originates from ground moraines (fine-grained stony

https://doi.org/10.5194/tc-2023-111
Preprint. Discussion started: 3 August 2023


The Cryosphere Discussions

tills) of the Late Wisconsin glacial episode (Duk-Rodkin and Lemmen, 2000) with some interceptions of alluvial, glaciofluvial and lacustrine deposits. The subsurface material is frequently ice-rich and consequently sensitive to climate change (Burn and Kokelj, 2009). The mean annual air temperature for 1990–2020 was $-7.1\,°C$ and $-8.9\,°C$ at Inuvik and Tuktoyaktuk, respectively (Environment and Climate Change Canada, 2021). The mean annual ground temperature ranges from approximately $-1\,°C$ in the taiga regions near Inuvik to approximately $-6\,°C$ in low-shrub tundra near Tuktoyaktuk (Kokelj et al., 2017). The permafrost thickness ranges from $100\,m$ near Inuvik to $500\,m$ in the northern parts of the study area (Mackay, 1967; Judge et al., 1979; Burn and Kokelj, 2009).

2.2 Methods objective 1: Snow accumulation at the embankment

To understand the influence of the road on the snow accumulation, we performed differencing between two elevation datasets, one snow-covered digital elevation model (further referred to as snow-covered DEM) and one snow-free digital terrain model (further referred to as snow-free DTM). For this analysis, we assumed that only the snow influences the elevation differences. We used a snow-free DTM by Lange et al. (2021), which was derived from airborne laser scanner (ALS) data with average point density of $11.93\,pts/m^2$ acquired on August 29, 2018 using a Riegl LMS-Q680i on board the Alfred-Wegener-Institute's (AWI) plane POLAR 5, a Basler BT-67 plane. The coordinate system for the snow-free DTM is WGS 1984, UTM 8N (EPSG 32608). The snow-free DTM has accuracy and precision levels of $0.03\,m$ and $0.05\,m$ respectively, both derived from global navigation satellite system (GNSS) measurements conducted during August 2018 (Lange et al., 2020). However, the snow-free DTM likely overestimates terrain elevation in areas of dense vegetation, leading to an underestimation of snow depth in those areas.

The snow-covered DEM was derived from a second ALS survey onboard the POLAR-5 science aircraft on April 10, 2019, representing the temporal window when the snowpack reaches its maximum depth during spring (Spark, 2023). The laser scanner was a Riegl VQ-580 which is specially designed to measure on snow and ice (Riegl, 2021). To create a DEM from the binary point-cloud data, we extracted the xyz-data and applied an atmospheric backscatter filter using the python-package awi-als-toolbox (Hendricks, 2019). We indexed and chunked the point clouds into tiles with a temporary buffer of $20\,m$ to avoid edge artifacts during the classification using LAStools. To distinguish ground points from non-ground points, we applied the Simple Morphological Filter (SMRF) (Pingel et al., 2013) using the Point Data Abstraction Library (PDAL). We interpolated the ground-classified dataset with inverse distance weighting (IDW) using the PointS2Grid approach integrated into PDAL with a circular neighbourhood search radius of $1.41\,m$. The format of the final gridded dataset was GeoTIFF with $1\,m$ cell size and the coordinate system WGS 1984, UTM 8N (EPSG 32608). The method what we have implemented for the ground classification and DEM generation is further described in Bookhagen (2018). In this study, we focused on the intersection of the two DEMs and the ITH spanning $4\,km$ of the highway (Fig. 1). We subtracted the snow-free DTM from the snow-covered DEM to obtain the snow depth distribution (Hammar et al., 2023) (submitted to PANGAEA).

We created $140\,m$ long transects (n = 4026) perpendicular to the road every $1\,m$ over the ITH centerline using GRASS GIS and extracted the snow depth values. Unfortunately, we did not have point measurements of snow depth to validate our data set. As an alternative approach to assess the accuracy of the snow depth raster, we used the transect sections over the road

https://doi.org/10.5194/tc-2023-111
Preprint. Discussion started: 3 August 2023

surface as a reference, assuming that it was free of snow and at the same elevation in both data sets. Consequently, the snow depth should be close to zero over the road. Our snow depth product has a high accuracy with a median snow depth of $<1\,\mathrm{cm}$ at the road surface and a standard variation of $5\,\mathrm{cm}$ (Fig. 2). Because of the high accuracy of the snow depth product, we did not perform any co-registration or shifting of the snow-covered DEM.

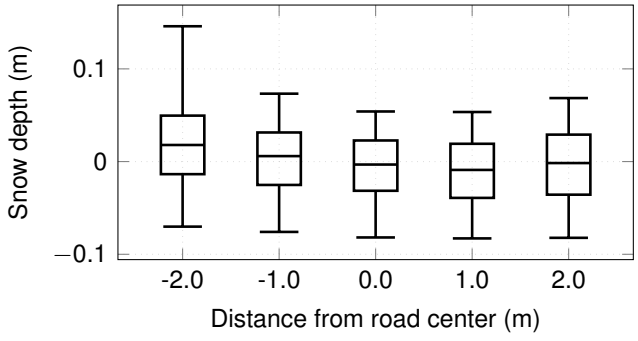

Figure 2. Snow depths derived from $5\,\mathrm{m}$ long transects across the road (n = 4026). The center lines indicate the median snow depth of all grid cells at a given distance from the approximate center location of the road, the box covers the 25th to 75th percentile and the whiskers the 5th to 95th percentile.

We assigned each transect an angle between $0\,^\circ$ to $180\,^\circ$ using the field calculator in QGIS. We categorized transects with angles $<45\,^\circ$ or $>135\,^\circ$ in relation to the north-south direction (n = 973), while those with angles within $45\,^\circ$ to $135\,^\circ$ were classified as in line with the east-west direction (n = 3053). In order to determine the embankment height, we required an elevation model without the embankment. For this, we clipped the snow-free DTM with a $10\,\mathrm{m}$ buffer around the centerline of the road, and interpolated the no data areas with a maximum search radius of $100\,\mathrm{m}$. Next, we subtracted this interpolated DTM from the initial DTM and determined the difference at the roads centerline for each transect. We divided the embankment heights into equal intervals and categorized them as low (n = 2051, $0.3\,\mathrm{m}$ to $0.9\,\mathrm{m}$), intermediate (n = 1335, $0.9\,\mathrm{m}$ to $1.4\,\mathrm{m}$), and high embankments (n = 640, $1.4\,\mathrm{m}$ to $2\,\mathrm{m}$). We analysed the snow depth distribution based on distance to the road center, cardinal direction and embankment height.

2.3 Methods objective 2: Road dust and snow albedo

To examine the temporal variation and the spatial extent to which the dust from the ITH affect the snow albedo we utilized 43 Sentinel-2 images between February 15 and May 30, 2020. We selected Sentinel-2 for this analysis because of the finer spatial resolution in the utilized bands ($10\,\mathrm{m}$ to $20\,\mathrm{m}$) as compared to Landsat ($30\,\mathrm{m}$). Surface snow albedo is affected by surface characteristics such as particle size, water content, impurity content, surface roughness, crystal orientation and structure (Zhang, 2005). Therefore, snow albedo can be strongly reduced by road dust. The broadband albedo is defined as the ratio of the reflected to the incident flux density from a unit surface area for the entire solar radiation spectrum ($300\,\mathrm{nm}$ to $3000\,\mathrm{nm}$) while narrowband albedo is the same ratio at a narrow range of wavelengths (Cogley et al., 2011). To obtain broadband albedo

https://doi.org/10.5194/tc-2023-111
Preprint. Discussion started: 3 August 2023

from satellite imagery, four steps are required (Traversa et al., 2021; Ren et al., 2021): (1) Cloud masking and atmospheric correction, which removes the scattering and absorption effects of atmospheric gasses and aerosols, (2) topographic correction, which corrects for the surface slope and aspect effects resulting in reflectance values that would be recorded over the equivalent horizontal surface (Wen et al., 2009), (3) anisotropy correction, which employs bidirectional reflectance distribution functions (BRDF) to correct for the anisotropic reflectance of a surface under varying illumintaion conditions, and (4) Narrowband to Broadband (NTB) conversion.

As we focused on relative differences in albedo and not on absolute values, we did not implement topographic or anisotropic corrections. We used atmospherically corrected Sentinel-2 data (bottom of atmosphere) available in Google Earth Engine (GEE). We pre-processed the Sentinel-2 using the GEE python application programming interface.

For cloud masking, we used the s2cloudless machine learning-based cloud detector developed by the Sentinel Hub research team, which uses cloud masks created by MAJA (Hagolle et al., 2017) as proxy for ground truth (Zupanc, 2019). Compared to other widely used cloud detection algorithms, s2cloudless has a high cloud detection rate and a lower misclassification rate of land and snow as clouds (Zupanc, 2021). Cloud probability for each pixel at $10\,\mathrm{m}$ scale is provided for every image in the Sentinel-2 archives in GEE, giving each image a corresponding s2cloudless image. The cloud probability is based on the pixel's Sentinel-2 band values (Zupanc, 2020) and the cloud shadow is defined by cloud projection intersection with low-reflectance near infrared (NIR) pixels (Miceli and Braaten, 2020). In this study, we applied the script by Miceli and Braaten (2020) with $40\,\%$ as threshold for cloud probability, 0.15 as threshold for NIR reflectance, a $50\,\mathrm{m}$ buffer to dilate the edge of cloud-identified objects and a maximum distance of $2\,\mathrm{km}$ to search for cloud shadows from cloud edges.

For the NTB conversion, we used the Liang et al. (2003) albedo formula. While it was initially developed for Landsat 5/7 data, it has been tested with the same empirical weighting parameters for the corresponding bands of Sentinel-2 (Naegeli et al., 2017). The formula provided good estimates for mean albedo values for glaciers (Naegeli et al., 2017) and thus, we expected the same performance for snow covered surfaces. The formula from Liang et al. (2003) adopted to the bands of Sentinel-2 (blue - b_2, red - b_4, NIR - b_8 and the two bands of shortwave infrared (SWIR); SWIR1 - b_{11} and SWIR2 - b_{12}) as suggested by Naegeli et al. (2017) is as follows:

$$\alpha_{\mathrm{Liang}} = 0.356\,b_2 + 0.130\,b_4 + 0.373\,b_8 + 0.085\,b_{11} + 0.072\,b_{12} - 0.0018 \tag{1}$$

To obtain the albedo from only the snow, we masked snow-free pixels and open water using the normalized difference snow index (NDSI) and normalized difference water index (NDWI), respectively. NDSI helps to discriminate snow, ice and water from bare soils and clouds (Dozier, 1989) by taking advantage of the high reflectance characteristics of snow and ice in the visible spectrum and the absorption in SWIR1. NDSI is defined as the difference between the green (b_3) and the SWIR1 (b_{11}) reflectance divided by their sum (Hall et al., 1995):

$$NDSI = \frac{b_3 - b_{11}}{b_3 + b_{11}} \tag{2}$$

Following Hall et al. (1995), ice, snow, and water were identified by a NDSI threshold value of >0.4, whereas bedrock and bare soils were identified by a value of <0.4. NDWI was proposed by McFeeters (1996) to delineate open water features. The

https://doi.org/10.5194/tc-2023-111
Preprint. Discussion started: 3 August 2023

index aims to use the green band to maximize the reflectance of the water body and the high absorption of NIR wavelengths to minimize it (McFeeters, 1996). It is defined as the difference between the green and NIR bands divided by their sum:

$$NDWI = \frac{b_3 - b_8}{b_3 + b_8} \quad (3)$$

To mask the open water, we applied a NDWI threshold of 0.4 which we determined based on visual interpretation.

For the pixel based analysis, we generated 120 buffers in $5\,\mathrm{m}$ intervals along the vectorized road, excluding the road and embankment. We extracted the snow albedo values in the buffer zones using the extract function in the eo-box Python package (Mack, 2018).

2.4 Methods objective 3: Spatial extent of early snow free areas

To determine how road dust affects the spatial extent of snowmelt, we assessed the fraction of snow-covered pixels along the corridor of the ITH with Landsat-7 and -8 imagery in May or June, when the landscape was still partly snow covered. We decided to use Landsat rather than Sentinel-2 because of the longer time series. We expected that even before road construction, the higher elevated and drier areas, which were chosen for the ITH, would, on average, have less snow cover than lower lying neighbouring terrain. To isolate the road effect, we compared imagery before (2002-05-17 and 2006-05-19, Landsat-7), during (2015-05-13, 2016-05-06 and 2017-05-18, Landsat-8) and after (2018-05-30, 2019-05-17 and 2020-05-26, Landsat-8) road construction. The imagery for these dates were cloud-free and showed a landscape that was partially covered with snow.

The snowmelt pattern analysis followed the workflow in Fig. 3. First, we calculated the NDSI for each image and created a snow mask. Second, we created a water mask using the NDWI of a snow-free image from August 2019 and applied it to all images to remove the water bodies. Using both masks, we divided all pixels into (I) snow-free ground, (II) snow and (III) water or ice. Last, we extracted the pixel categories and the pixel coordinates in a $1000\,\mathrm{m}$ buffer zone from the road using the extract function in the eo-box Python package (Mack, 2018). With the pixel coordinates we calculated the distance of every pixel to the road edge using the QGIS tool "distance to nearest hub". To obtain percent snow cover we divided the pixels that were classified as snow by the total number of land pixel per $5\,\mathrm{m}$ distance along the entire $138\,\mathrm{km}$ road.

The total snow cover observed in the Landsat images varies across the different years, due to multiple contributing factors such as photo timing and climate variability, making it difficult to compare the road effect between the years. To focus on the road effect exclusively, we normalized the snow cover by calculating the snow cover average for each year at distances between $900\,\mathrm{m}$ to $1000\,\mathrm{m}$. At this distance, it is reasonable to posit that the impact of the road is negligible (Everett, 1980; Ackerman and Finlay, 2019). We used this average value as a normalizing value, and divided each snow cover value by this value.

3 Results

3.1 Snow accumulation at the embankment

The ITH embankment increased snow accumulation on both sides of the road (Fig. 4a). The region of enhanced snow accumulation reached up to $36\,\mathrm{m}$ from the road center at north facing embankment slopes with the strongest accumulation at $10\,\mathrm{m}$

https://doi.org/10.5194/tc-2023-111
Preprint. Discussion started: 3 August 2023

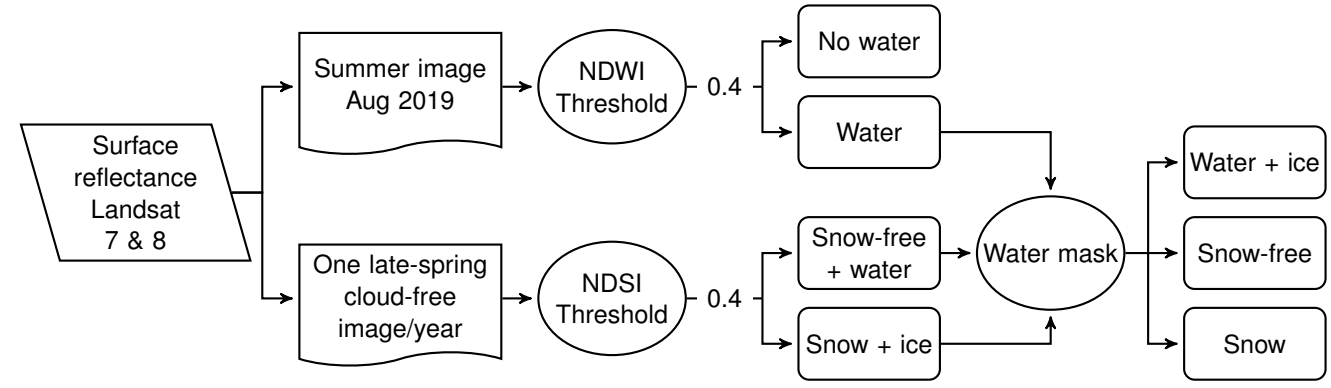

Figure 3. Processing chain for snow discrimination using Landsat data.

to 26 m (Fig. 4a). Within this 16 m distance, we found a median snow depth up to 0.92 m, representing the maximum median value observed within the 1 m increments on the transects. In south direction, we measured enhanced snow accumulation up to 20 m from the road center and the median snow depth within the strongest accumulation zone (between 9 m to 14 m) was up to 0.88 m (Fig. 4a). Furthermore, the median snow depth farther away from the road was generally greater on the northern side (0.5 m) than on the southern side (0.3 m). As shown by the 25th–75th percentiles, the snow depth variability increased with increasing snow accumulation for both sides. The snow depth variability was generally larger on the northern side than the southern side. Moreover, the northern side showed a double peak in snow depths as represented by the 75th percentiles compared to the southern side that showed one snow depth peak.

As compared to north-south direction, more transects in the study area were located in east-west direction (n=973 versus n=3053). Enhanced snow accumulation reached up to 36 m and 25 m from the road center at the western and eastern side, respectively (Fig. 4a). We found the deepest snow within a distance of 10 m to 20 m from the road center on the western side (median snow depth up to 1.09 m) and a distance of 10 m to 16 m on the eastern side (median snow up to 0.97 m).

The snow accumulation characteristics varied with embankment height (Fig. 4b). The snow accumulation enhancement for all embankment heights reached distances up to 36 m (Fig. 4b) from the road center. For low embankments (ranging from 0.3 m to 0.9 m) the median snow depth was up to 1.03 m at the embankment toe. For intermediate embankments heights (0.9 m to 1.4 m) the median snow depth was up to 1.16 m and the variation in snow depth was more pronounced at greater distances from the road compared to other embankment heights. The higher embankments, measuring 1.4 m to 2 m in height at the studied road segments exhibited a median snow depth of up to 1.32 m.

At the Trail Valley Creek research station close to the study area, the predominant wind direction between October 2018 and April 2019 was south (Fig. 4c). This period corresponds to the winter months preceding snow depth data acquisition. Eastern and western wind directions occurred approximately equally often, but wind from the east was, on average, stronger. Relative to the typical meteorological conditions recorded between 1998 and 2021, easterly winds were more frequent during the study period (Environment and Climate Change Canada, 2021).

https://doi.org/10.5194/tc-2023-111
Preprint. Discussion started: 3 August 2023

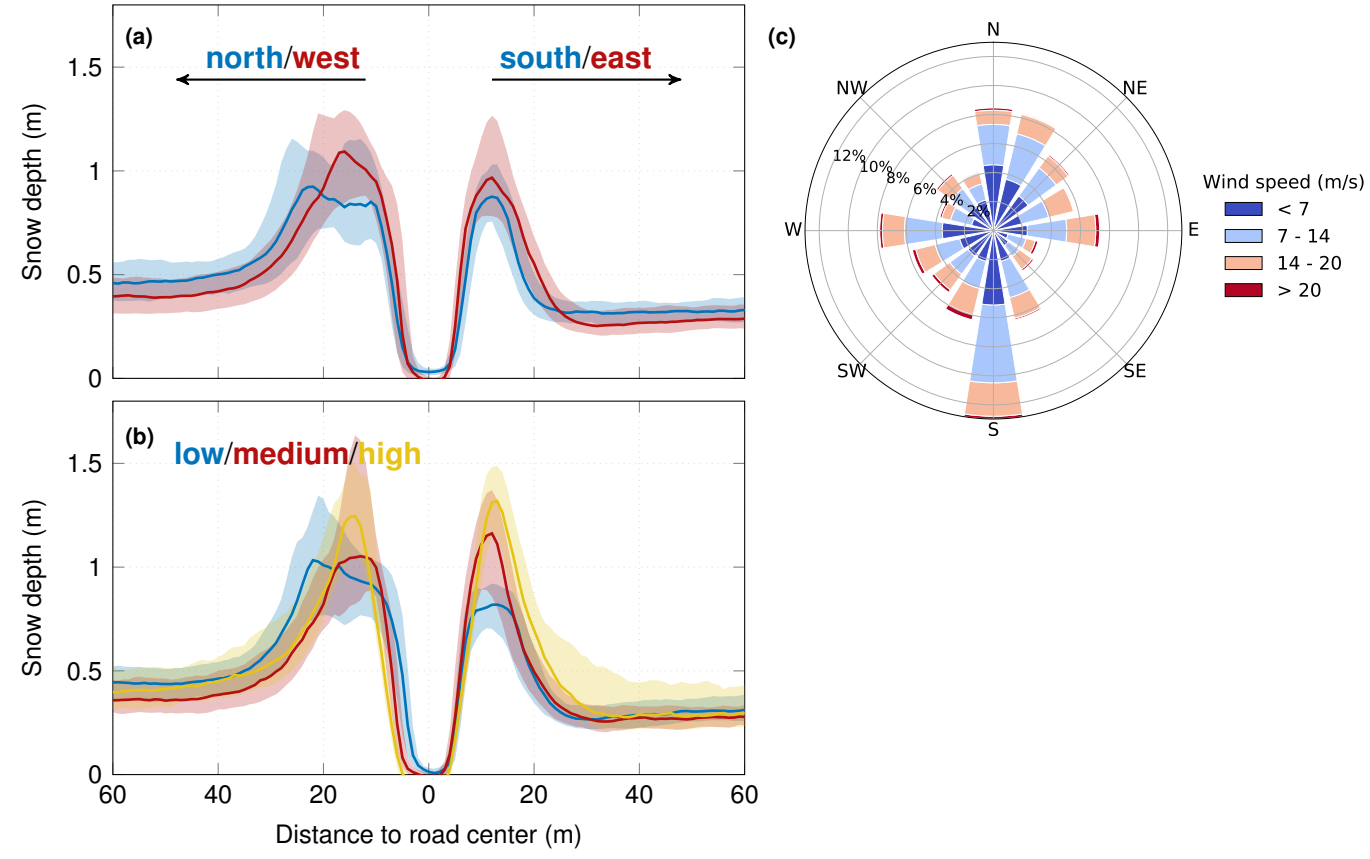

Figure 4. Snow accumulation derived from n = 4026 transects across the road at (a) north - south (n = 973, blue) and east - west (n = 3053, red) facing embankment slopes and at (b) low (n = 2051, 0.3 m to 0.9 m, blue), intermediate (n = 1335, 0.9 m to 1.4 m, red), and high embankments (n = 640, 1.4 m to 2 m, yellow). The coloured lines indicate the median snow depth of all grid cells at a given distance from the approximate center location of the road, the shades represent the 25th–75th percentiles. (c) shows the predominant wind direction for the Trail Valley Creek study site (October 2018 – April 2019).

3.2 Snow albedo decrease

We found that during the snowmelt period, the snow albedo decreased earlier in areas close to the road as compared to 500 m away (Fig. 5a,c). Before 5 April, snow albedo was similar at all distances from the road embankment edge ranging from 0.5 to 0.83 for different dates. From April 5 to May 8, snow albedo close to the road was already decreasing, while snow albedo at more than 200 m distance remained high. The largest difference of snow albedo by distance to the road was around May 13, when the closest pixels (20 m distance) showed snow albedo values of only 0.45 while albedo at 900 m from the road was around 0.7. Afterwards, the variation gradually decreased again but consistently followed the same pattern, with the closest distance to the road edge displaying the lowest albedo values and the farthest distance showing the highest values.

https://doi.org/10.5194/tc-2023-111
Preprint. Discussion started: 3 August 2023

The Cryosphere
Discussions
Open Access
EGU

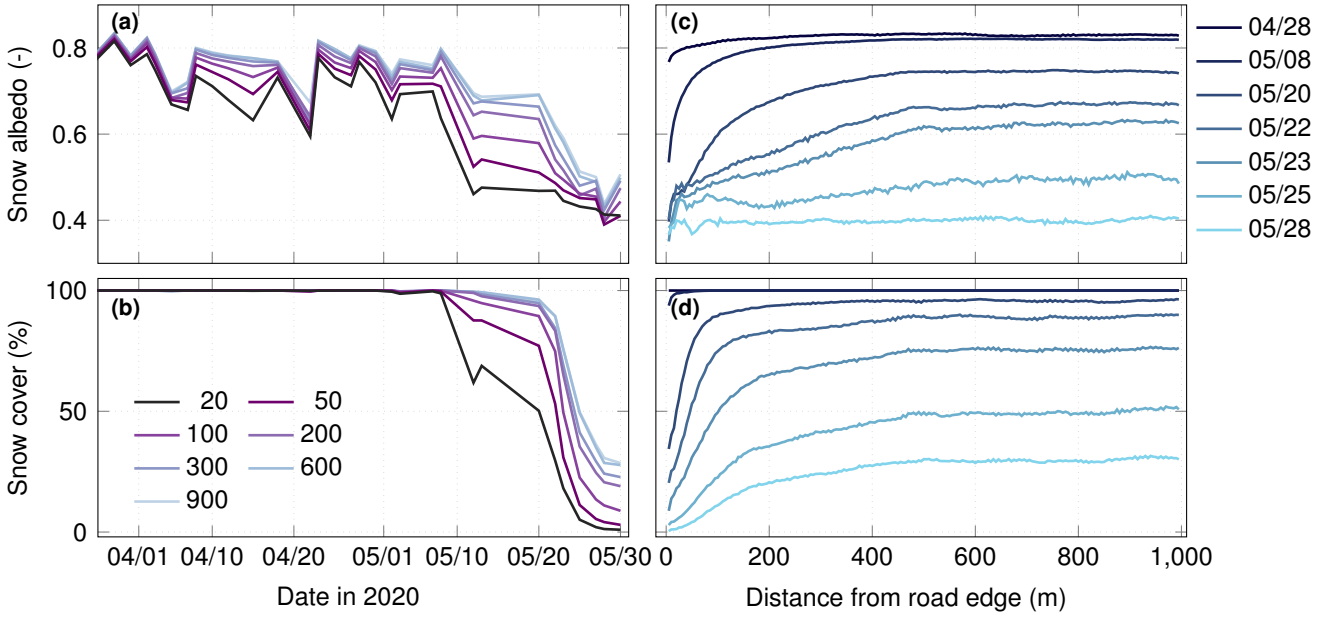

Figure 5. Snow albedo and snow cover fraction for Sentinel-2 pixels of a certain distance to the road embankment edge for March 27 to May 30, 2020; (a) time series of average snow albedo for seven distances, (b) time series of percentage of snow covered pixels for seven distances, (c) median snow albedo for seven selected dates and (d) percentage of snow covered pixels for seven selected dates.

The study area was fully snow covered throughout the winter until May 8 (Fig. 5b, derived from the NDSI). In the following two weeks, the snow cover close to the road decreased drastically. Areas far away from the road edge (500 m to 900 m) remained almost fully snow covered until May 20. Thereafter, the snow melted fast and at May 30, undisturbed areas showed a snow coverage of 30 %. Close to the road, the snow started to melt twelve days earlier than at distances farther away and on May 30 the area nearby the road was snow-free. The onset of the snowmelt for the distances 50 m and 100 m was similar as for 20 m but the rate was slower and more area remained snow-covered at May 30 as compared to 20 m from the road edge (Fig. 5b). Areas more than 500 m from the road edge do not reveal decreasing snow albedo or earlier melt than at 1000 m distance (Fig. 5c–d).

https://doi.org/10.5194/tc-2023-111
Preprint. Discussion started: 3 August 2023

The Cryosphere
Discussions
Open Access
EGU

3.3 Spatial extent of early snow free areas

We found that snow close to the road melted earlier. As an example, this is illustrated in Fig. 6a–b, which shows a true color composite and a section of the classified landscape from a Landsat-8 image from May 30, 2018.

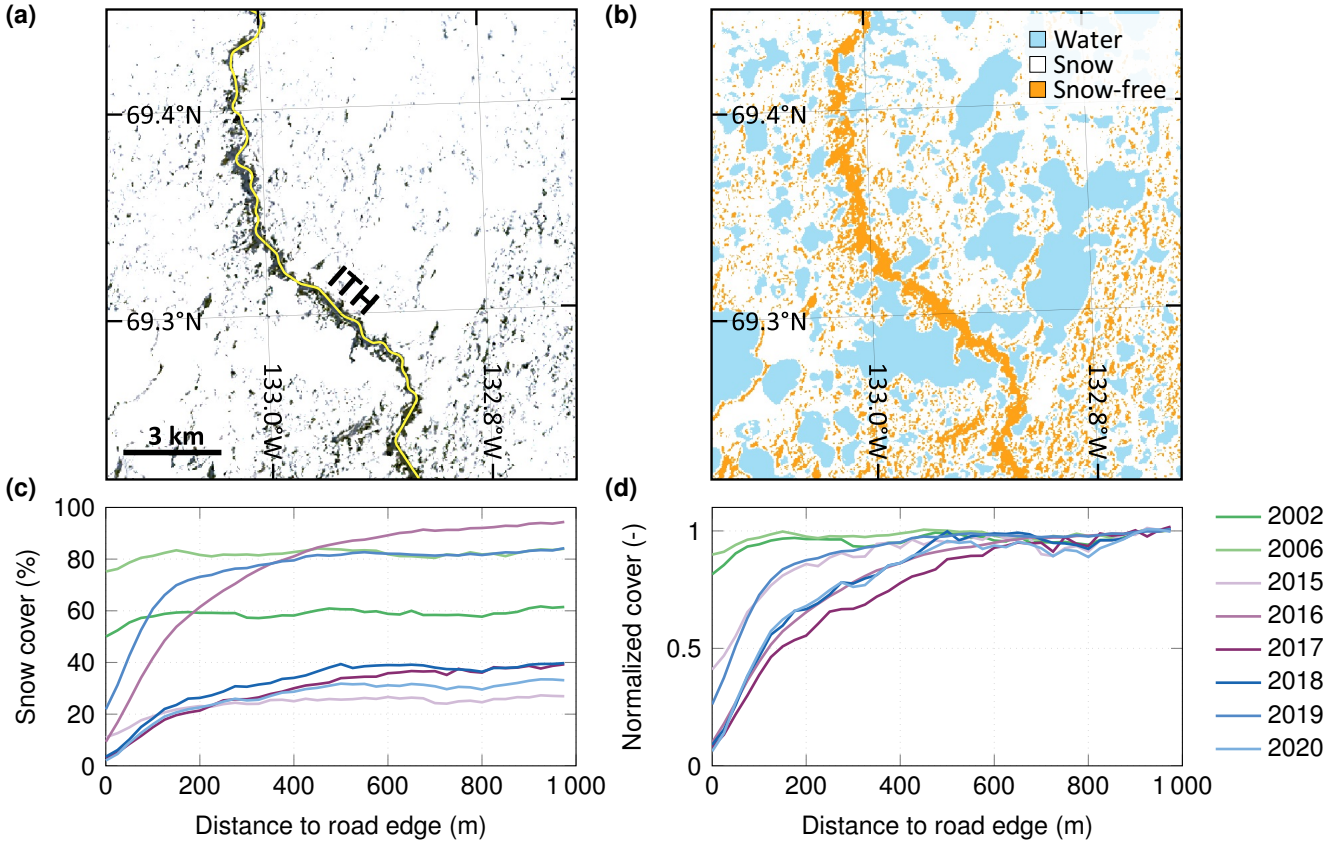

Figure 6. (a) a true color composite of a partly melted landscape (May 30, 2018, Landsat-8 image), (b) classified landscape with snow-covered areas (white), snow-free areas (orange) and the water bodies (blue) which were masked using an NDWI threshold on a Landsat-8 image of late summer, (c) presence of snow with distance from ITH derived from Landsat-7 and -8 images using NDSI and (d) relative snow cover as fraction of the value far away from the road (900 m to 1000 m). The images before road construction were from May 17, 2002 and May 19, 2006, during construction from May 13, 2015, May 6, 2016 and May 18, 2017 and after construction from May 30, 2018, May 17, 2019, May 26, 2020. (a) and (b) depict an example section of the study area (area highlighted in orange in Fig. 1), while (c) and (d) show data from the entire 138 km long road.

In general, the selected images captured during the snowmelt consistently revealed lower snow cover in proximity of the road, including the imagery before construction (2002 and 2006, green in Fig. 6c–d). However, the magnitude of this effect differed between the time before construction and other years. The images from 2002 and 2006 showed a homogeneous snow

https://doi.org/10.5194/tc-2023-111
Preprint. Discussion started: 3 August 2023

cover pattern of the study area of 60% and 80%, respectively. The variation of snow cover with distance was almost identical for the images before construction years despite the differences in absolute snow cover values. We observed a gradual decrease towards the (at that time not yet constructed) road of approximately $5\,\%$ to $10\,\%$ at distances starting at $100\,\mathrm{m}$ from the road for both years. Furthermore, the snow cover pattern of the year 2015, which corresponds to the period when the quarries were established but not the primary road, exhibited similar shape to the preceding years.

In 2016, the construction of the road had a strong impact on the snowmelt pattern. Nearly the entire landscape farther from the road was snow covered in the May 6, 2016 image ($80\,\%$ to $90\,\%$). Still, the area in the vicinity of the road was almost snow-free. The snowmelt patterns in the imagery from 2017, 2018 and 2020 were similar, both in shape and absolute values of snow cover. The snow cover decreased from about $20\,\%$ ($\pm 5\,\%$) at a distance of $150\,\mathrm{m}$ from the road edge to $5\,\%$ in road vicinity. At distances between $500\,\mathrm{m}$ and $150\,\mathrm{m}$ from the road edge, there was a gradual decrease from $30\,\%$ ($\pm 5\,\%$) to $20\,\%$ ($\pm 5\,\%$) while snow cover showed stable values beyond $500\,\mathrm{m}$. Although the image from 2019 showed a larger total snow cover than 2017, 2018 and 2020, the road effect was similar. A gradual decline became apparent at a distance of $500\,\mathrm{m}$ towards the road and the largest road effects occurred within the first $150\,\mathrm{m}$.

To compare the snow cover of the two sides of the road, we subtracted the percentage of snow cover on the road's eastern side from its western side (not shown). Of all the years, only 2016 had a large difference in snow cover fraction between the eastern and western sides of the road. In the 2016 image, the western side showed less snow cover at all distances, with largest differences at distances between $50\,\mathrm{m}$ to $500\,\mathrm{m}$. In other years, the difference between the two sides fluctuated around zero (± 10 percent points).

The impact of the road on the snow cover becomes more evident when it is compared to undisturbed areas after normalization (Fig. 6d). A normalized snow cover value of 1 indicates that the snow cover at a given distance to the road is comparable to the undisturbed reference areas. All Landsat images exhibited values close to 1 beyond distances of $600\,\mathrm{m}$ from the road edge, indicating a state of similarity with undisturbed areas. The images from before the construction (2002 and 2006) remained around the value of 1 at closer distances, indicating an undisturbed state. The strongest differences in snow cover compared to the undisturbed region occurred within distances of $150\,\mathrm{m}$ from the road edge for the images from during and after construction. We observed the effects of the road as the onset of a negative trend in normalized snow cover at $400\,\mathrm{m}$ and $600\,\mathrm{m}$ for the years 2015/2019 and 2016–2018/2020, respectively.

4 Discussion and outlook

4.1 Snow accumulation at the embankment

Snow depth estimates from airborne data along transects across the road revealed enhanced snow accumulation at both sides of the road. This result is in line with other studies based on manual snow surveys (Benson et al., 1975; O'Neill and Burn, 2017). O'Neill and Burn (2017) manually measured the snow depths along transects in tundra and forest at the Peel Plateau at the Dempster Highway (Northwest Territories, Canada) and found an enhanced snow accumulation at the embankment in the tundra landscape. They noted a significant enhancement at a distance of about $5\,\mathrm{m}$ to $15\,\mathrm{m}$ from the side of the road and then

https://doi.org/10.5194/tc-2023-111
Preprint. Discussion started: 3 August 2023

a decrease. Manual snow surveys are very labour intensive. Therefore, the study by O'Neill and Burn (2017) includes only six transects in tundra and a maximum distance of 50 m to the road. In contrast, the remote sensing data enabled us to analyse more than 4000 transects of up to 70 m from the road center. The large number of transects allows patterns of variation and controls to be explored over larger areas. In this way, we showed that a gradual increase of snow accumulation reached as far as 36 m away from the road center. The differences in enhanced snow accumulation compared to (O'Neill and Burn, 2017) may be attributed to different methodology, precipitation, wind-regimes, vegetation and terrain geometry.

In general, snow accumulation at the embankment can be caused by snow plowing and additional snow collection when the embankment acts as a wind break. While we expect snow plowing to enhance snow accumulation equally on both sides and irrespective of the embankment shape, wind induced accumulation is likely affected by the local conditions. Based on the findings of Benson et al. (1975) and Liston and Sturm (1998) and the prevailing southern winds (Fig. 4c), enhanced snow accumulation in the lee of the road towards the north can be expected. This was confirmed by our results (Fig. 4a). The transects in north direction (leeward side) showed more snow accumulation reaching up to 36 m from the road center as compared to 20 m at the southern side. At our specific location, the more strongly enhanced snow accumulation at the northern side could also be induced by the topographic location of the transects. For the road sections studied, the north-facing side was generally located at higher elevations than the south-facing side. At a distance of 60 m from the road, the elevation towards the road decreased by an average of 1.4 m. Close to the embankment, the slope suddenly changed due to the construction, which can cause turbulence and snow deposition.

In the east-west direction, the frequency and average wind speed were similar with slightly stronger winds from the east (Fig. 4c). The similar frequency of wind directions was reflected in the snow accumulation for the transects in east-west direction, which showed similar snow depth patterns on both sides in contrast to north-south facing embankments (Fig. 4a). However, for the transects in west direction, the snow accumulation reached distances farther away from the road center. But also here the topography may play an important role as the western side was located at higher elevation compared to the eastern side. Another possibility is that events of very strong winds, which are more frequent for wind from the east, have a disproportionally large effect on snow redistribution.

For the road sections in our snow accumulation analysis (4 km of the total 138 km length), we had a wide range of embankment heights available, ranging from 0.3 m to 2 m. With this, we showed that the embankment height influenced the magnitude of the snow accumulation. The embankments that we classified as high had, on average, 0.3 m deeper snow as compared to low embankments (Fig. 4b). The high embankments are used on road sections with particularly vulnerable ice-rich permafrost to prevent the underlying permafrost from thawing (Kiggiak - EBA, 2011). However, due to increased snow accumulation, high embankments are one factor within the complex feedback system that could potentially contribute to the degradation of permafrost. The low embankments, on the other hand, also had more snow accumulated compared to distances farther away. One important contributing factor to this extra snow accumulation is likely the snow plowing. Typically, low embankments with gentle slopes should facilitate a laminar flow of wind, enabling it to blow the snow away (Lanouette et al., 2015).

It should be noted that our snow accumulation results only represent road sections in the tundra landscape. The snow accumulation along the embankment is probably less further south along the road where trees provide shelter and prevent snow

https://doi.org/10.5194/tc-2023-111
Preprint. Discussion started: 3 August 2023

drifting (O'Neill and Burn, 2017) and may also vary further north. Notwithstanding these limitations, these results give us a better understanding of the spatial distribution of snow next to a permafrost road embankment.

Snow accumulation was identified as one of the key factors contributing to permafrost degradation and increased thaw depths along infrastructure (Park et al., 2015; Schneider von Deimling et al., 2021). The insulating properties of deep snow lead to warmer ground temperatures in winter, thus increases the thickness of the active layer (Gouttevin et al., 2012). In addition, the increased snow accumulation serves as an additional source of water when the snow melts, contributing to higher soil moisture and pond formation along the embankment in the spring and delaying soil refreezing in autumn due to latent heat release (Zhang, 2005). The spatial pattern of snow distribution remains stable from year to year (Sturm and Wagner, 2010). Therefore, the map of snow distribution and snow depth we produced could be integrated into permafrost degradation and blowing snow models and contribute to their validation and improvement.

4.2 Snow albedo decrease

We provided the first Sentinel-2 derived snow albedo time series along the ITH for the year 2020. We found similar snow albedo values at all distances from the road until April 5, 2020 (Fig. 5). This indicates that frequent new snowfalls in winter cover the deposited dust. Moreover, a protective layer of snow or ice on the road may shield the dust from mobilization. After April 5, we showed that the snow albedo was lower at distances close to the road and higher at distances farther away. This may be due to dust accumulation at the snow surface when snow melts and settles. We detected road related effects on the snow albedo up to $500\,\mathrm{m}$ from the road. In contrast, snow albedo at $600\,\mathrm{m}$ and $900\,\mathrm{m}$ from the road showed similar values and temporal patterns across whole study period and therefore indicated little or no effect of the road at these distances. Moreover, the snow cover fraction decreased earlier at closer distances to the road as compared to farther away. At $20\,\mathrm{m}$ distance, the melt-off started May 8, 2020 while it started twelve days later at $600\,\mathrm{m}$ distance. This finding is in line with Benson et al. (1975) who described a two weeks premature snowmelt along roads in Prudhoe Bay region, Alaska, due to dust lowering the snow albedo.

4.3 Spatial extent of early snow free areas

We examined the snowmelt patterns along the road using the NDSI derived from Landsat data. Even though snow accumulates near the road, these areas are melting earlier than regions farther away in spring (Fig. 6). Most of the enhanced snow accumulation is within $30\,\mathrm{m}$ as shown in Fig. 4, which is also the spatial resolution of the Landsat bands used for calculating the NDSI. Therefore, even if the snow in the absolute vicinity of the road persists longer because of greater snow depth, it may not be visible in the images because of the spatial resolution of the utilized sensor.

The results are in line with other similar studies showing earlier snowmelt next to a gravel road on permafrost in Prudhoe Bay, Alaska (Bergstedt et al., 2022). However, unlike their study we could not identify any considerable effect when classifying the pixels depending on the side of the road. A possible explanation is that the majority of the road is located in north-south direction and the prevailing wind direction in winter 2018–2018 was from the south (Fig. 4f). The eastern and western winds are similar in wind speed and occurrence which may explain why we did not find substantial differences between the sides.

https://doi.org/10.5194/tc-2023-111
Preprint. Discussion started: 3 August 2023

Furthermore, we classified the landscape west and east of the road and did not consider short sections of the road which are in east-west direction.

Other studies have identified road dust as the main cause of the early melt-off in spring (Everett, 1980; Walker and Everett, 1987). Dust loading on snow leads to decreased snow albedo and, thus, increased absorption of solar energy, inducing snowmelt. Everett (1980) showed that most dust falls within a distance of 300 m with a logarithmic decrease with distance. This finding is in accordance with the spatial pattern of snow melt found in our work (Fig. 5b,d and 6c–d). This was especially clear in the images from the years 2016 and 2019, representing a high snow cover farther away from the road (90% and 80%), while the area close to the road was already mostly snow-free.

We detected earlier snowmelt at distances up to 600 m from the road depending on the observation date, which is greater than in previous studies. The main snowmelt extent in this study was within a zone of 200 m whereas Benson et al. (1975) noted that the early snowmelt occurred primarily within a 100 m zone (along roads in the Prudhoe Bay region). One possible explanation for the differences in snowmelt may be the misclassification of the NDSI when the snow is contaminated with dust and thus falsely classified as snow-free. However, the reliability of the NDSI given different spectral characteristics of the snow was examined in Kulkarni et al. (2002). They found that the NDSI values for all types of snow, such as fresh, clean, patchy and wet and contaminated were substantially different from snow-free areas. A second explanations for the differences in snowmelt extent may be different wind speeds, dust particle size and snow clearance practices. Furthermore, our method may be more sensitive to small effects as we analyse thousands of satellite pixels.

We found reduced snow cover along the road also in the images before construction. This can be attributed to the road being constructed in interfluvial regions and at elevated terrain, which typically exhibits lower snow accumulation than lower lying areas and topographic hollows. As a result, these areas experience an earlier and more frequent absence of snow compared to other parts of the landscape.

Permafrost is affected by the early melt-off in multiple ways. Auerbach et al. (1997) found the deepest thaw next to the Dalton Highway (Alaska) and a consistent decrease with distance from the road. They attributed the increased thaw depth close to the road to the earlier exposure to solar radiation. The melt-off can start up to 14 days before the general melt-off (Walker and Everett, 1987), which can affect the underlying vegetation. Vegetation phenology and start of the season are significantly correlated with the last day of snow cover as found in Zeng and Jia (2013). Some plants are more favored by early snowmelt than others, as noted in Auerbach et al. (1997). They highlighted the close relationship between early snowmelt and vascular plant growth, deciduous shrub and sedge flowering. Tall shrubs may act as a windbreak, increasing dust deposition and snow accumulation, leading to more soil nutrients, higher soil temperatures and increased active layer thickness (Gill et al., 2014). Our results indicate, that dust deposition is the main driver of the early snowmelt and the lower snow albedo at distances closer to the road. The affected footprint may be larger than earlier believed and even if there is currently no evidence for permafrost degradation at such distances, these seeming undisturbed areas may be affected in the future.

https://doi.org/10.5194/tc-2023-111
Preprint. Discussion started: 3 August 2023

4.4 Conclusion

In this study, we utilized remote sensing techniques to show enhanced snow accumulation, reduced snow albedo and the extent of earlier snowmelt following the construction of the ITH. Our study confirms that the presence of the road significantly affects snow accumulation, resulting in enhanced snow accumulation up to $36\,\mathrm{m}$ from the road. High embankments result in deeper snow, but also low embankments with gentle slopes contribute to enhanced snow accumulation, which can potentially contribute to permafrost degradation. The observed decrease in snow albedo and earlier snowmelt near roads have significant implications for permafrost stability and ecosystem dynamics. The impacts of road infrastructure on snow albedo reached $500\,\mathrm{m}$ and the extent of earlier snowmelt up to $600\,\mathrm{m}$ from the road, highlighting the far-reaching influence of roads on the surrounding environment. Understanding the effects of snow road interactions in permafrost areas is crucial for current management practices and future development of mitigation strategies. Our results contribute to a better understanding of road effects on snow, a potential driver of permafrost degradation. These snow effects are most pronounced locally, but we show effects up to seemingly undisturbed areas at greater distance to the road. Furthermore, we recommend increased monitoring of dust deposition along Arctic highways and further research on remote sensing techniques to gain a better understanding of the impacts of road infrastructure on tundra vegetation and the surrounding environment. These efforts will contribute to informed decision-making and the preservation of permafrost stability in the face of infrastructure development and maintenance during during a time of unprecedented climate warming.

Author contributions. J.H. designed the study and led the manuscript preparation. I.G. and J.B. initiated and supervised the study and advised on the methodology. All authors interpreted the results and contributed to the text of the manuscript.

Competing interests. The authors declare that they have no competing interests.

Code and data availability. The snow covered DEM and snow depth product is submitted and will be available in PANGAEA.

Acknowledgements. We thank the AWI IceBird team for the 2019 overflight over the ITH, providing us with essential airborne LiDAR data and Timothy Ensom for pointing us to related research by the Northern Territory Geological Survey (NTGS) and providing valuable input. Part of this work [Jennika Hammar/Inge Grünberg] was funded by Helmholtz Imaging, a platform of the Helmholtz Incubator on Information and Data Science [grant number: ZT-I-PF-4-001]. The authors also acknowledge that this study was conducted in the Inuvialuit settlement region in the western Canadian Arctic.

https://doi.org/10.5194/tc-2023-111
Preprint. Discussion started: 3 August 2023

References

Ackerman, D.: Shrub-induced snowpack variability alters wintertime soil respiration across a simulated tundra landscape, Polar Research, 37, https://doi.org/10.1080/17518369.2018.1468197, 2018.

Ackerman, D. E. and Finlay, J. C.: Road dust biases NDVI and alters edaphic properties in Alaskan arctic tundra, Scientific Reports, 9, 1–8, https://doi.org/10.1038/s41598-018-36804-3, 2019.

Auerbach, N. A., Walker, M. D., and Walker, D. A.: Effects of roadside disturbance on substrate and vegetation properties in Arctic tundra, Ecological Applications, 7, 218–235, 1997.

Benson, C., Holmgren, B., Timmer, R., Weller, G., and Parrish, S.: Observations on the seasonal snow cover and radiation climate at Prudhoe Bay, Alaska during 1972, Ecological investigations of the tundra biome in the Prudhoe Bay region, Alaska. Biological Papers of the University of Alaska, Special report, pp. 12–50, 1975.

Bergstedt, H., Jones, B. M., Walker, D. A., Peirce, J. L., Bartsch, A., Pointner, G., Kanevskiy, M. Z., Raynolds, M. K., and Buchhorn, M.: The spatial and temporal influence of infrastructure and road dust on seasonal snowmelt, vegetation productivity, and early season surface water cover in the Prudhoe Bay Oilfield, Arctic Science, pp. 1–26, https://doi.org/10.1139/as-2022-0013, 2022.

Biskaborn, B. K., Smith, S. L., Noetzli, J., Matthes, H., Vieira, G., Streletskiy, D. A., Schoeneich, P., Romanovsky, V. E., Lewkowicz, A. G., Abramov, A., Allard, M., Boike, J., Cable, W. L., Christiansen, H. H., Delaloye, R., Diekmann, B., Drozdov, D., Etzelmüller, B., Grosse, G., Guglielmin, M., Ingeman-Nielsen, T., Isaksen, K., Ishikawa, M., Johansson, M., Johannsson, H., Joo, A., Kaverin, D., Kholodov, A., Konstantinov, P., Kröger, T., Lambiel, C., Lanckman, J. P., Luo, D., Malkova, G., Meiklejohn, I., Moskalenko, N., Oliva, M., Phillips, M., Ramos, M., Sannel, A. B. K., Sergeev, D., Seybold, C., Skryabin, P., Vasiliev, A., Wu, Q., Yoshikawa, K., Zheleznyak, M., and Lantuit, H.: Permafrost is warming at a global scale, Nature Communications, 10, 1–11, https://doi.org/10.1038/s41467-018-08240-4, 2019.

Bookhagen, B.: Pre-process and classify lidar or SfM point-cloud data for processing with PC_geomorph_roughness, https://github.com/BodoBookhagen/PC_geomorph_roughness/blob/master/docs/PC_geomorph_roughness_manual.pdf, 2018.

Brandt, J.: The extent of the North American boreal zone, Environmental Reviews, 17, 101–161, https://doi.org/10.1139/A09-004, 2009.

Burn, C. R. and Kokelj, S. V.: The environment and permafrost of the Mackenzie Delta area, Permafrost and Periglacial Processes, 20, 83–105, https://doi.org/https://doi.org/10.1002/ppp.655, 2009.

Cameron, E. A. and Lantz, T. C.: Drivers of tall shrub proliferation adjacent to the Dempster Highway, Northwest Territories, Canada, Environmental Research Letters, 11, https://doi.org/10.1088/1748-9326/11/4/045006, 2016.

Cogley, J., Hock, R., Rasmussen, L., Arendt, A., Bauder, A., Braithwaite, R., Jansson, P., Kaser, G., Möller, M., Nicholson, L., and Zemp, M.: Glossary of glacier mass balance and related terms, vol. 86 of *IHP-VII Technical Documents in Hydrology*, UNESCO-IHP, https://doi.org/10.5167/uzh-53475, 2011.

Darrow, M. M.: Thermal modeling of roadway embankments over permafrost, Cold Regions Science and Technology, 65, 474–487, https://doi.org/10.1016/j.coldregions.2010.11.001, 2011.

Dozier, J.: Spectral signature of alpine snow cover from the landsat thematic mapper, Remote Sensing of Environment, 28, 9–22, https://doi.org/https://doi.org/10.1016/0034-4257(89)90101-6, 1989.

Duk-Rodkin, A. and Lemmen, D.: Glacial history of the Mackenzie region, in: The Physical Environment of the Mackenzie Valley, Northwest Territories: a Baseline for the Assessment of Environmental Change, edited by Dyke, L. and Brooks, G., vol. 547, pp. 11–20, Geological Survey of Canada, 2000.

Environment and Climate Change Canada: Historical Climate Data, URL: https://climate.weather.gc.ca/, accessed: 2021-07-15, 2021.

Everett, K. R.: Distribution and properties of road dust along the northern portion of the Haul Road, in: Environmental engineering and ecological baseline investigations along the Yukon River-Prudhoe Bay Haul Road, edited by Brown, J. and Berg, R., chap. 3, pp. 101–128, Publisher: U.S. Army Cold Regions Research and Engineering Laboratory, 1980.

Fortier, R., LeBlanc, A. M., and Yu, W.: Impacts of permafrost degradation on a road embankment at Umiujaq in Nunavik (Quebec), Canada, Canadian Geotechnical Journal, 48, 720–740, https://doi.org/10.1139/t10-101, 2011.

Fraser, R. H., Lantz, T. C., Olthof, I., Kokelj, S. V., and Sims, R. A.: Warming-Induced Shrub Expansion and Lichen Decline in the Western Canadian Arctic, Ecosystems, 17, 1151–1168, https://doi.org/10.1007/s10021-014-9783-3, 2014.

Ge, Y. and Gong, G.: Land surface insulation response to snow depth variability, Journal of Geophysical Research Atmospheres, 115, 1–11, https://doi.org/10.1029/2009JD012798, 2010.

Gill, H. K., Lantz, T. C., O'Neill, B., and Kokelj, S. V.: Cumulative impacts and feedbacks of a gravel road on shrub tundra ecosystems in the Peel Plateau, Northwest Territories, Canada, Arctic, Antarctic, and Alpine Research, 46, 947–961, https://doi.org/10.1657/1938-4246-46.4.947, 2014.

Gouttevin, I., Menegoz, M., Dominé, F., Krinner, G., Koven, C., Ciais, P., Tarnocai, C., and Boike, J.: How the insulating properties of snow affect soil carbon distribution in the continental pan-Arctic area, Journal of Geophysical Research: Biogeosciences, 117, 1–11, https://doi.org/10.1029/2011JG001916, 2012.

Government of Canada: Infrastructure Canada Projects and Programs (since 2002) - Northwest Territories, URL: https://www.infrastructure.gc.ca/investments-2002-investissements/nt-eng.html, accessed: 2021-08-15, 2021.

Gädeke, A., Langer, M., Boike, J., Burke, E. J., Chang, J., Head, M., Reyer, C. P. O., Schaphoff, S., Thiery, W., and Thonicke, K.: Climate change reduces winter overland travel across the Pan-Arctic even under low-end global warming scenarios, Environmental Research Letters, 16, 024 049, https://doi.org/10.1088/1748-9326/abdcf2, 2021.

Hagolle, O., Huc, M., Desjardins, C., Auer, S., and Richter, R.: MAJA Algorithm Theoretical Basis Document, https://doi.org/10.5281/zenodo.1209633, 2017.

Hall, D. K., Riggs, G. A., and Salomonson, V. V.: Development of methods for mapping global snow cover using moderate resolution imaging spectroradiometer data, Remote Sensing of Environment, 54, 127–140, https://doi.org/https://doi.org/10.1016/0034-4257(95)00137-P, 1995.

Hammar, J., Grünberg, I., Hendricks, S., Jutila, A., Helm, V., and Boike, J.: Snow covered digital elevation model and snow depth product (2019), Trail Valley Creek, NWT, Canada, https://doi.org/tba, 2023.

Hendricks, S.: AWI ALS toolbox, URL: https://github.com/shendric/awi-als-toolbox.git, accessed: 2021-08-15, 2019.

Idrees, M., Burn, C., Moore, J., and Calmels, F.: Monitoring permafrost conditions along the Dempster Highway, in: GeoQuébec 2015: challenges from North to South, 2015.

Judge, A. S., Taylor, A. E., and Burgess, M.: Canadian Geothermal Data Collection–Northern Wells 1977–1978, 1979.

Kiggiak - EBA: Environmental impact statement for construction of the Inuvik to Tuktoyaktuk highway, NWT, EIRB File No. 02/10-05, 2011.

Kokelj, S. V., Palmer, M. J., Lantz, T. C., and Burn, C. R.: Ground Temperatures and Permafrost Warming from Forest to Tundra, Tuktoyaktuk Coastlands and Anderson Plain, NWT, Canada, Permafrost and Periglacial Processes, 28, 543–551, https://doi.org/10.1002/ppp.1934, 2017.

Kulkarni, A. V., Srinivasulu, J., Manjul, S. S., and Mathur, P.: Field based spectral reflectance studies to develop NDSI method for snow cover monitoring, Journal of the Indian Society of Remote Sensing, 30, 73–80, https://doi.org/10.1007/BF02989978, 2002.

https://doi.org/10.5194/tc-2023-111
Preprint. Discussion started: 3 August 2023

Lange, S., Cable, W. L., Grünberg, I., and Boike, J.: GNSS measurements Inuvik-Tuktoyaktuk-Highway (ITH) and Trail Valley Creek (TVC) 2018, https://doi.org/10.1594/PANGAEA.918649, 2020.

Lange, S., Grünberg, I., Anders, K., Hartmann, J., Helm, V., and Boike, J.: Airborne Laser Scanning (ALS) point clouds of the Inuvik-Tuktuyaktuk-Highway, NWT, Canada (2018), https://doi.org/10.1594/PANGAEA.939655, 2021.

Lanouette, F., Doré, G., Fortier, D., and Lemieux, C.: Influence of snow cover on the ground thermal regime along an embankment built on permafrost : In-situ measurements, 68e Conférence Canadienne de Géotechnique et 7e Conférence Canadienne sur le Pergélisol, 20 au 23 septembre 2015, Québec., https://doi.org/10.13140/RG.2.1.2482.1848, 2015.

Liang, S., Shuey, C. J., Russ, A. L., Fang, H., Chen, M., Walthall, C. L., Daughtry, C. S., and Hunt, R.: Narrowband to broadband conversions of land surface albedo: II. Validation, Remote Sensing of Environment, 84, 25–41, https://doi.org/10.1016/S0034-4257(02)00068-8, 2003.

Lievens, H., Brangers, I., Marshall, H.-P., Jonas, T., Olefs, M., and De Lannoy, G.: Sentinel-1 snow depth retrieval at sub-kilometer resolution over the European Alps, The Cryosphere, 16, 159–177, https://doi.org/10.5194/tc-16-159-2022, 2022.

Liston, G. E. and Sturm, M.: A snow-transport model for complex terrain, Journal of Glaciology, 44, 498–516, https://doi.org/10.3189/S0022143000002021, 1998.

Macander, M. J., Swingley, C. S., Joly, K., and Raynolds, M. K.: Landsat-based snow persistence map for northwest Alaska, Remote Sensing of Environment, 163, 23–31, https://doi.org/10.1016/j.rse.2015.02.028, 2015.

Mack, B.: Sentinel-2 Cloud Masking with s2cloudless, URL: https://github.com/benmack/eo-box.git, accessed: 2021-09-15, 2018.

Mackay, J.: The Mackenzie Delta Area, N.W.T., Canada, Queen's printer, 1963.

Mackay, J. R.: Permafrost Depths, Lower Mackenzie Valley, Northwest Territories, Arctic, 20, 21–26, https://doi.org/https://doi.org/10.14430/arctic3275, 1967.

McFeeters, S. K.: The use of the Normalized Difference Water Index (NDWI) in the delineation of open water features, International Journal of Remote Sensing, 17, 1425–1432, https://doi.org/10.1080/01431169608948714, 1996.

Miceli, J. and Braaten, J.: Sentinel-2 Cloud Masking with s2cloudless, URL: https://github.com/google/earthengine-community/tree/master/tutorials/sentinel-2-s2cloudless, accessed: 2021-09-15, 2020.

Morse, P. D. and Wolfe, S. A.: Geological and meteorological controls on icing (aufeis) dynamics (1985 to 2014) in subarctic Canada, Journal of Geophysical Research: Earth Surface, 120, 1670–1686, https://doi.org/https://doi.org/10.1002/2015JF003534, 2015.

Naegeli, K., Damm, A., Huss, M., Wulf, H., Schaepman, M., and Hoelzle, M.: Cross-Comparison of Albedo Products for Glacier Surfaces Derived from Airborne and Satellite (Sentinel-2 and Landsat 8) Optical Data, Remote Sensing, 9, 110, https://doi.org/10.3390/rs9020110, 2017.

Nelson, F. E., Anisimov, O. A., and Shiklomanov, N. I.: Subsidence risk from thawing permafrost, Nature, 410, 889–890, https://doi.org/10.1038/35073746, 2001.

Nill, L., Grünberg, I., Ullmann, T., Gessner, M., Boike, J., and Hostert, P.: Remote Sensing of Environment Arctic shrub expansion revealed by Landsat-derived multitemporal vegetation cover fractions in the Western Canadian Arctic, Remote Sensing of Environment, 281, 113 228, https://doi.org/10.1016/j.rse.2022.113228, 2022.

O'Neill, H. B. and Burn, C. R.: Impacts of variations in snow cover on permafrost stability, including simulated snow management, Dempster Highway, Peel Plateau, Northwest Territories, Arctic Science, 3, 150–178, https://doi.org/10.1139/as-2016-0036, 2017.

Park, H., Fedorov, A. N., Zheleznyak, M. N., Konstantinov, P. Y., and Walsh, J. E.: Effect of snow cover on pan-Arctic permafrost thermal regimes, Climate Dynamics, 44, 2873–2895, https://doi.org/10.1007/s00382-014-2356-5, 2015.

https://doi.org/10.5194/tc-2023-111
Preprint. Discussion started: 3 August 2023

Pingel, T. J., Clarke, K. C., and McBride, W. A.: An improved simple morphological filter for the terrain classification of airborne LIDAR data, ISPRS Journal of Photogrammetry and Remote Sensing, 77, 21–30, https://doi.org/https://doi.org/10.1016/j.isprsjprs.2012.12.002, 2013.

Rampton, V.: Quaternary Geology of the Tuktoyaktuk Coastlands, Northwest Territories, Commission géologique du Canada. Memoir, Publisher: Energy, Mines and Resources Canada, https://books.google.de/books?id=LqFsnQAACAAJ, 1988.

Rantanen, M., Karpechko, A. Y., Lipponen, A., Nordling, K., Hyvärinen, O., Ruosteenoja, K., Vihma, T., and Laaksonen, A.: The Arctic has warmed nearly four times faster than the globe since 1979, Communications Earth & Environment, 3, 168, https://doi.org/10.1038/s43247-022-00498-3, 2022.

Raynolds, M. K., Walker, D. A., Ambrosius, K. J., Brown, J., Everett, K. R., Kanevskiy, M., Kofinas, G. P., Romanovsky, V. E., Shur, Y., and Webber, P. J.: Cumulative geoecological effects of 62 years of infrastructure and climate change in ice-rich permafrost landscapes, Prudhoe Bay Oilfield, Alaska, Global Change Biology, 20, 1211–1224, https://doi.org/10.1111/gcb.12500, 2014.

Ren, S., Miles, E. S., Jia, L., Menenti, M., Kneib, M., Buri, P., McCarthy, M. J., Shaw, T. E., Yang, W., and Pellicciotti, F.: Anisotropy parameterization development and evaluation for glacier surface albedo retrieval from satellite observations, Remote Sensing, 13, https://doi.org/10.3390/rs13091714, 2021.

Riegl: Airborne laser scanner with online waveform processing, URL: http://www.riegl.com/uploads/tx_pxpriegldownloads/DataSheet_VQ-580_2015-03-23.pdf, accessed: 2021-10-15, 2021.

Schneider von Deimling, T., Lee, H., Ingeman-Nielsen, T., Westermann, S., Romanovsky, V., Lamoureux, S., Walker, D. A., Chadburn, S., Trochim, E., Cai, L., Nitzbon, J., Jacobi, S., and Langer, M.: Consequences of permafrost degradation for Arctic infrastructure – bridging the model gap between regional and engineering scales, The Cryosphere, 15, 2451–2471, https://doi.org/10.5194/tc-15-2451-2021, 2021.

Spark, W.: Average Monthly Snowfall in Inuvik, URL: https://weatherspark.com/y/292/Average-Weather-in-Inuvik-Canada-Year-Round#Figures-Snowfall, accessed: 2023-04-21, 2023.

Sturm, M. and Wagner, A. M.: Using repeated patterns in snow distribution modeling: An Arctic example, Water Resources Research, 46, https://doi.org/https://doi.org/10.1029/2010WR009434, 2010.

Traversa, G., Fugazza, D., Senese, A., and Frezzotti, M.: Landsat 8 OLI broadband albedo validation in Antarctica and Greenland, Remote Sensing, 13, 1–19, https://doi.org/10.3390/rs13040799, 2021.

van der Sluijs, J., Kokelj, S. V., Fraser, R. H., Tunnicliffe, J., and Lacelle, D.: Permafrost terrain dynamics and infrastructure impacts revealed by UAV photogrammetry and thermal imaging, Remote Sensing, 10, https://doi.org/10.3390/rs10111734, 2018.

Van der Sluijs, J., Saiet, S., Bakelaar, C., Wentworth, A., Fraser, R., , and Kokelj, S.: Beyond visual-line-of-sight (BVLOS) drone operations for environmental and infrastructure monitoring: a case study in northwestern Canada, Drone Systems and Applications, 2023 in press.

Walker, B., Wilcox, E. J., and Marsh, P.: Accuracy assessment of late winter snow depth mapping for tundra environments using structure-from-motion photogrammetry, Arctic Science, 7, 588–604, https://doi.org/10.1139/as-2020-0006, 2021.

Walker, D. A. and Everett, K. R.: Road dust and its environmental impact on Alaskan taiga and tundra, Arctic & Alpine Research, 19, 479–489, https://doi.org/10.2307/1551414, 1987.

Walker, D. A., Raynolds, M. K., Kanevskiy, M. Z., Shur, Y. S., Romanovsky, V. E., Jones, B. M., Buchhorn, M., Jorgenson, M. T., Šibík, J., Breen, A. L., Kade, A., Watson-Cook, E., Bergstedt, H., Liljedahl, A. K., Daanen, R. P., Connor, B., Nicolsky, D., and Peirce, J. L.: Cumulative impacts of a gravel road and climate change in an ice-wedge polygon landscape, Prudhoe Bay, AK, Arctic Science, 27, 1–27, https://doi.org/10.1139/as-2021-0014, 2022.

https://doi.org/10.5194/tc-2023-111
Preprint. Discussion started: 3 August 2023

Wen, J., Liu, Q., Liu, Q., Xiao, Q., and Li, X.: Parametrized BRDF for atmospheric and topographic correction and albedo estimation in Jiangxi rugged terrain, China, International Journal of Remote Sensing - INT J REMOTE SENS, 30, 2875–2896, https://doi.org/10.1080/01431160802558618, 2009.

Wilcox, E. J., Keim, D., de Jong, T., Walker, B., Sonnentag, O., Sniderhan, A. E., Mann, P., and Marsh, P.: Tundra shrub expansion may amplify permafrost thaw by advancing snowmelt timing, Arctic Science, 5, 202–217, https://doi.org/10.1139/as-2018-0028, 2019.

Zeng, H. and Jia, G.: Impacts of snow cover on vegetation phenology in the arctic from satellite data, Advances in Atmospheric Sciences, 30, 1421–1432, https://doi.org/10.1007/s00376-012-2173-x, 2013.

Zhang, T.: Influence of the seasonal snow cover on the ground thermal regime: An overview, Reviews of Geophysics, 43, https://doi.org/10.1029/2004RG000157, 2005.

Zupanc, A.: Improving Cloud Detection with Machine Learning, URL: https://medium.com/sentinel-hub/improving-cloud-detection-with-machine-learning-c09dc5d7cf13, accessed: 2021-09-15, 2019.

Zupanc, A.: Cloud Masks at Your Service, URL: https://medium.com/sentinel-hub/cloud-masks-at-your-service-6e5b2cb2ce8a, accessed: 2021-09-15, 2020.

Zupanc, A.: Sentinel Hub Cloud Detector, URL: https://www.sentinel-hub.com/sites/default/s2cloudless.pdf, accessed: 2021-09-15, 2021.